Strain-Aware Performance Evaluation and Correction for OTFT-Based Flexible Displays

Tengtao Li and Sachin S. Sapatnekar
ECE Department, University of Minnesota, Minneapolis, MN 55455
e-mail: {lixx2967, sachin}@umn.edu

***Abstract*—Organic thin-film transistors (OTFTs) are widely used in flexible circuits, such as flexible displays, sensor arrays, and radio frequency identification cards (RFIDs), because these technologies offer features such as better flexibility, lower cost, and easy manufacturability using low-temperature fabrication process. This paper develops a procedure that evaluates the performance of flexible displays. Due to their very nature, flexible displays experience significant mechanical strain/stress in the field due to the deformation caused during daily use. These deformations can impact device and circuit performance, potentially causing a loss in functionality. This paper first models the effects of extrinsic strain due to two fundamental deformations modes, bending and twisting. Next, this strain is translated to variations in device mobility, after which analytical models for error analysis in the flexible display are derived based on the rendered image values in each pixel of the display. Finally, two error correction approaches for flexible displays are proposed, based on voltage compensation and flexible clocking.**

I. Introduction

Flexible electronics are built using bendable, elastic, and lightweight materials. Flexible circuits are often implemented using organic semiconductor materials and permit significant strain when a deformation is induced in the structure. These technologies are amenable to low-cost roll-to-roll manufacturing techniques, can be conformally shaped, and can be used to construct large-area structures [1]. As a result, they are being increasingly deployed in flexible displays [2], flexible sensor arrays [3], radio frequency identification cards (RFIDs) [4], electronic paper, and system-in-foil (SiF) [5].

Organic thin-film transistors (OTFTs) offer an attractive technology for flexible circuits. OTFT circuits [6] have been demonstrated to implement ring oscillators, decoders, flip-flops, pulse-generators, voltage multipliers, charge amplifiers, etc. Several applications of OTFTs, including flexible displays [2], sensor arrays [3], [7], RFIDs [4] and organic DRAM cells [8] have been reported. The speed of these systems lags that of cutting-edge CMOS, but they can provide the right level of performance in applications where flexibility is paramount. In flexible displays, the OTFT acts as a switch driving a capacitance in each pixel, which is charged to a voltage that renders an appropriate bias to the display cell [2]. For organic DRAM cells [8], the OTFT acts as a switch during read/write operations.

In this paper, we consider the application area of flexible displays and focus on designing displays that, in addition to showing mechanical integrity under strain, are also resilient to the performance variation caused by extrinsic strain. Specifically, we show how the electrical characteristics of the circuitry may be affected by strain (e.g., through shifts in device carrier mobilities due to piezoresistance), which may influence the functional correctness of the system.

A flexible display, shown in Fig. 1 [5], consists of multiple layers: a) a *flexible substrate* (composed of materials such as polyimide (PI), plastic, or even paper), which provides mechanical support for other layers; b) a *matrix backplane* comprising a layer of devices that control the display, driven by row/column drivers, as detailed at the top right of the figure; c) a *functional display layer* with an $n \times m$ liquid crystal matrix, each pixel of which is controlled by the voltage level of a separate storage capacitor; d) a *front transparent plane* that provides protection and isolation from air, water, and dust.

[0]This work was supported in part by the NSF under award CCF-1421606.

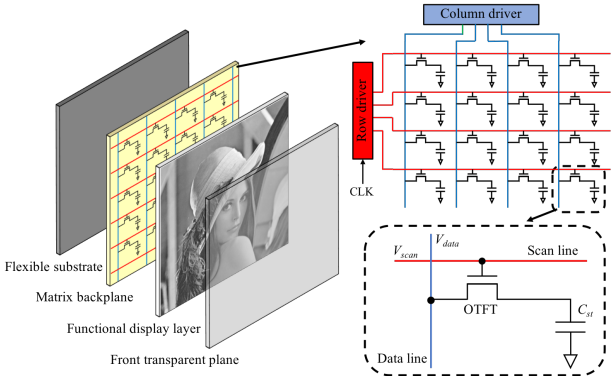

Fig. 1: Structure of a liquid crystal flexible display with OTFTs.

The flexible display is periodically refreshed at a rate that is in the order of μs (at these rates, OTFTs switching speeds are fast enough), with all n pixel rows activated one by one using a shift register. The OTFT is turned on by activating the row/scan line, and the storage capacitor is charged/discharged through the column/data line. The voltage of the storage capacitor determines the pixel value of each display pixel. For a grayscale display, the pixel value ranges from 0 to 255, while a color display uses three sub-pixels in each pixel, each with a value ranging from 0 to 255, representing RGB values of the pixel. This work focuses on grayscale images, with 8-bit pixel values, but the concepts can be extended easily to RGB images.

As compared to conventional CMOS technologies, OTFTs involve a simpler manufacturing process based on low-cost deposition of thin films of semiconducting organic materials on flexible substrates at relatively low temperature. The mechanical flexibility of OTFTs makes them compatible with flexible substrate for lightweight and foldable products [9]. However, these advantages come at a performance penalty: typical mobility values in OTFT devices range from 0.1–1 cm^2/Vs for organic devices, with the best organic materials achieving mobility of 1–10 cm^2/Vs [9], [10]. Flexible displays are subject to changes in shape, which can be modeled using several modes: bending, pressing, and twisting [11]–[13]. The influence of strain on the mobility, on-current and leakage current of an individual OTFT device is discussed in [14], but to our knowledge, there is no work that clearly evaluates the effect of strain on a typical OTFT application. As we will show, the strain induced by these deformations may have a significant influence on the quality of the image in a flexible display.

The contribution of this paper is to analyze the performance variations of flexible displays due to strain, and to rectify the errors induced due to this variation. The work is conducted in three steps:

(a) Strain analysis due to bending, twisting, and pressing.
(b) Analysis of OTFT carrier mobility degradation analysis under strain, and its translation to the error in the displayed image.
(c) Error correction using two approaches: voltage compensation and the use of a flexible clock.

II. Strain Modeling of a Flexible Display

A. Basic Principles

Strain is a measure of deformation, representing the displacement between particles in an object relative to a reference length. The mechanical strain field can be represented as the tensor:

$$\epsilon = \epsilon_{ij} = \begin{pmatrix} \epsilon_{11} & \epsilon_{12} & \epsilon_{13} \\ \epsilon_{21} & \epsilon_{22} & \epsilon_{23} \\ \epsilon_{31} & \epsilon_{32} & \epsilon_{33} \end{pmatrix} \quad (1)$$

where the subscripts $i, j \in \{1, 2, 3\}$ refer to the three coordinate axes, ϵ_{ii} are normal strains, and $\epsilon_{ij,i\neq j}$ are shear strains.

Stress physically corresponds to the reactionary internal forces per unit due to deformation of an object under external forces. The mechanical stress field can also be represented by a tensor:

$$\sigma = \sigma_{ij} = \begin{pmatrix} \sigma_{11} & \tau_{12} & \tau_{13} \\ \tau_{21} & \sigma_{22} & \tau_{23} \\ \tau_{31} & \tau_{32} & \sigma_{33} \end{pmatrix} \quad (2)$$

where the subscripts $i, j \in \{1, 2, 3\}$ refer to the three coordinate axes, σ_{ii} are normal stresses, and τ_{ij} are shear stresses. Within the elastic limit, stress and strain are related by Hooke's law.

B. Strain Analysis of a Flexible Display

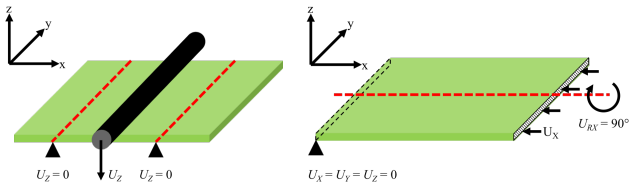

(a) Bend (b) Twist+press

Fig. 2: FEA simulation set up for two types of deformations.

We conduct finite element analysis (FEA) simulations for the flexible display under various types of deformations using ABAQUS, from which the strain and stress can be obtained and then translated to device variations. The dimensions of the flexible display used in our FEA simulation are 50mm × 50mm × 0.5μm (length × width × thickness). The display contains 512 × 512 pixels and the corresponding resolution is 260 ppi. The material of the structure is polyimide (PI), which is widely used for the substrate of flexible displays, and its thickness is 500μm. The Young's modulus of PI is 2.5GPa and the Poisson's ratio equals to 0.34 [15]. In this FEA simulation structure, we omit the device layer, located near the top of the substrate, for two reasons: first, because the OTFT layer is very flexible by design, and second, because its thickness is much lower than the thickness of the substrate [15].

During the daily use of the flexible display, it may suffer various of deformations, such as bending, twisting, pressing/stretching. Manufactured systems are typically stress-tested to determine their response to such deformations [16], [17]. We now show the boundary conditions (BCs) for FEA simulations for two typical deformations.

Bend: The FEA simulation is for bend deformation is set up as shown in Fig. 2(a). The plane in green is the top view of the flexible display which is made of PI. First, the BC $U_Z = 0$ is applied to the two red dotted lines, where U_Z denotes the displacement along the z-axis. This BC is used to fix the two red dotted lines along the z-axis, but it allows the lines slide in the x-y plane during the bend process. Then a rigid beam in the shape of cylinder is placed on the top of the display and is used to bend the display. The BC U_Z along the negative z-axis is applied to the beam and then the display is bent by the beam. When U_Z is large enough value, the bend radius is approximately equal to the radius of the cylindrical rigid beam.

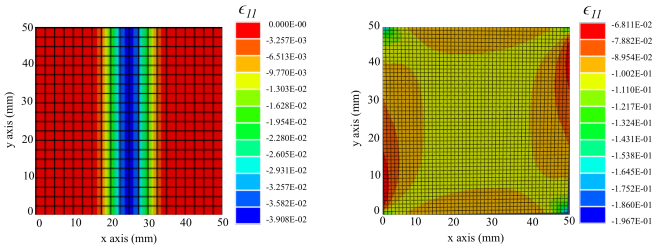

(a) Bend (b) Twist+press

Fig. 3: FEA simulation results of Fig. 2 showing strain distributions.

Twist+press: Figure 2(b) illustrates the set-up for the FEA simulation for the twist+press deformation. First, the left y-z surface of the display is fixed. Then a BC $U_{RX} = 90°$ is applied to the right y-z surface of the display, where U_{RX} donates the rotational degree of freedom along the x-axis. As a result, the surface is rotated by 90° along the red dotted line, which is located at the center of the display and is parallel to the x-axis. Meanwhile, another BC U_X is applied to the same surface along the negative x-axis. With this BC, the display is pressed along the x-axis.

The results of FEA simulation showing the strain induced by these two deformations on the top surface, corresponding to the location of the device layer, are displayed in Fig. 3. A negative sign represents compressive strain, while a positive value donates tensile strain. A rigid beam with a radius of 5mm is used to bend the display in this simulation, similar to typical values used for bending tests [18]. In this case the strain on the top surface is negative (compressive); on the other hand, the bottom surface (not shown) experiences an equal and opposite positive (tensile) strain. Under normal bending conditions, strains change gradually in space. Similarly, Fig. 3(b) shows the ϵ_{11} result induced by the twist+press deformation. In this simulation, two BCs, $U_X = -5$mm and $U_{RX} = 90°$ are applied to the display.

Unlike the bend deformation, which causes compressive strain in the upper layer and tensile strain in the lower layer (not shown), in these simulations, the twist+press deformation induces compressive strain only, all through the display structure (if the press deformation is lower, tensile strain can also be seen). Reversing the BC direction to $U_X = +5$mm along the positive x-axis results in tensile strain.

Based on the contours in Fig. 3, this twist+press deformation can induce much more significant strain in the display than the bend deformation described here; as a result, it will cause more significant influence on the OTFT devices and thus on the entire display.

III. Mobility Variation Due to Strain

The structure of a single OTFT is illustrated in Fig. 4, and shows one bottom gate electrode buried in the gate dielectric material and another two electrodes, source and drain, on the top. Organic semiconductor material is placed between the top contacts and dielectric layer and the current in the channel is controlled by the voltage applied to the gate electrode [9], [10].

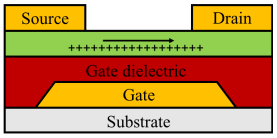

Fig. 4: The structure of a bottom-gate top-contact OTFT.

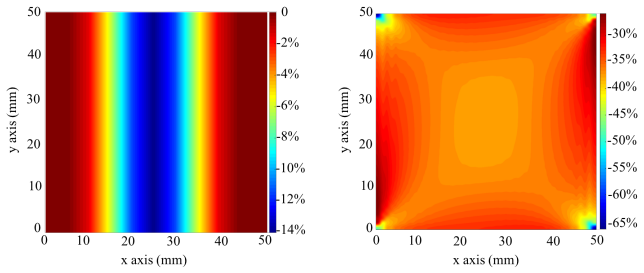

(a) Bend (b) Twist+press

Fig. 5: Mobility variation results for two types of deformations.

The OTFTs considered in this paper are based on conjugated molecular systems with alternating single and double carbon-carbon bonds, and their molecular p-bonding orbitals are responsible for the ability of the material to transport charge [19], [20]. Regioregular poly(3-hexylthiophene) (P3HT) is a type of alkyl-substituted polythiophenes, which have have excellent solubility in a variety of organic solvents, and thin films are readily prepared by spin-coating, dip-coating, drop-coating, screen printing, or inkjet printing [10]. Stable doping of P3HT has been realized by adding strong molecular acceptors, such as 2,3,5,6-tetrafluoro7,7,8,8-tetracyanoquinodimethane (F_4TCNQ), which can undergo efficiently hole transfer for P3HT. Thus, the P3HT-based OTFT is a p-type device [21].

TABLE I: The strain-mobility relationship in P3HT OTFT [14]

ϵ_{11} (%)	0.42	0.84	1.26	1.75	1.98	2.45
$\Delta\mu/\mu$ (%)	2.80	4.20	5.60	7.20	7.90	9.50

slope = 3.3 [no units, since it is a ratio of two percentages]

According to piezoresistive theory, mechanical deformation changes the electrical resistivity of the semiconductor material [14], [22]. In transistors, the strain affects the mobility of the carriers and as a result the drain current and the speed of the transistor. The relationship between the relative change in mobility and strain is shown in Table I [14]. The slope of the fitted linear relationship between the relative change in mobility and strain is 3.3. In other words, a tensile strain with the value of 1% will cause a 3.3% increase in P3HT OTFT, while a compressive strain with the value of -1% will cause 3.3% mobility degradation in OTFT. It can be shown that P3HT based OTFTs have a good mechanical flexibility, the sensitivity between mobility variation and strain can reach a much higher value of 26 using alternative methods for building flexible electronics using amorphous silicon based inorganic TFTs [23].

The mobility variation results for the two types of deformations in Section II are shown in Fig. 5. Since the bend deformation and twist+press deformation both induce compressive strain with negative sign, the devices will suffer mobility degradation in both deformations. As shown in Fig. 5(a), the bend deformation can cause a mobility degradation up to -14%, and the maximum degradation occurs at the center. The twist+press deformation will induce larger mobility degradation because it will induce more significant compressive strain. The maximum mobility degradation occurs near the corner and even the average mobility degradation can reach -36%.

IV. Performance Evaluation of Flexible Displays

Each pixel of the display contains a capacitor charged through an OTFT switch, as shown in Fig. 1. The whole display frame is refreshed periodically with a specific system-defined refresh frequency. The frame refresh period t_f is the time interval in which the refresh operation for the whole display should be completed, and is the reciprocal of the refresh frequency [1]. Since each refresh operation activates the n_{row} rows in the display in sequence, the row refresh period, t_{row}, is given by:

$$t_{row} = t_f / n_{row} \tag{3}$$

All pixels in the row are refreshed simultaneously.

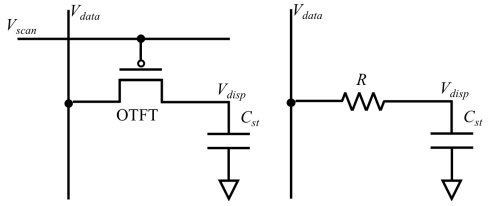

(a) Pixel circuit (b) RC model

Fig. 6: (a) An OTFT in a pixel and (b) its equivalent RC model [1].

A circuit representation of each pixel is shown in Fig. 6. Here, V_{data} and V_{scan} represent the voltage level of data and scan lines, respectively. The p-type OTFT switch, controlled by V_{scan}, allows access to the storage capacitor, C_{st}, whose charge reflects the pixel value. In each step, C_{st} stores the pixel value at the current moment. This can be altered when the OTFT is turned ON through V_{scan}, when the voltage level of C_{st} is changed to new pixel value by charging/discharging the capacitor such that:

$$t_{\text{charge/discharge}} \leq t_{row} \tag{4}$$

where $t_{\text{charge/discharge}}$ is the time required to charge/discharge C_{st} to V_{data} successfully. If (4) is not satisfied, then the process of charging/discharging C_{st} may be incomplete, and errors may be induced into the pixel values. In such a display, with 512 rows, at a refresh frequency of 120Hz, from (3), the refresh period $t_{row} = 16.3\mu$s represents the time to complete charge/discharge for every pixel.

As discussed in Sections II and III, the deformations in a flexible display induce strain. In OTFTs, compressive strain causes mobility degradation due to the piezoresistive effect. Since the charge/discharge current through the OTFT is proportional to the device mobility, strain-induced mobility degradation will reduce the charge/discharge current, necessitating a longer time for C_{st} to reach accurate pixel value. The range of $V_{DD} = 1$V is distributed across 256 pixel values, so that each grayscale level corresponds to 3.9mV. Assuming an allowable noise margin of half a level, charging is complete when the pixel value is $\pm$1.95mV of the final value.

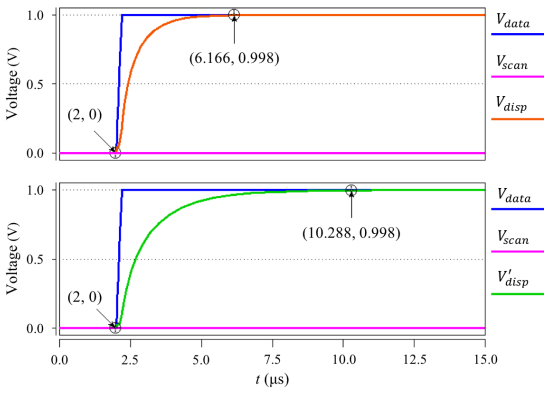

Fig. 7: V_{disp} transients at the nominal and a shifted mobility value.

We perform HSPICE simulations to determine V_{disp}, the voltage across C_{st} that is provided to the liquid crystal display pixel, for

the circuit in Fig. 6(a). The OTFT device model is provided by the Organic Process Design Kit (OPDK) [24], a design kit that was specifically developed for OTFTs. We use a corner-based model for the transistor to capture the worst-case impact of process variations. Fig. 7 shows the transient voltage across C_{st} as it charges from a pixel value of 0 (0V) to 255 (1V). The transient at the nominal (strain-free) mobility value, denoted by V_{disp}, is shown in the upper curve, and has a charging period of 4.166μs after V_{data} switches at 2μs. The same operation under a 50% mobility degradation is shown by the lower plot in the V'_{disp} curve, and is seen to require a significantly longer period of 8.288μs.

Note that if the voltage in the upper curve is examined before 4.166μs, it will provide an approximation to the final value. In some cases, this approximation may be adequate and may be invisible to the user, but in other cases, it may corrupt the image significantly. The image is inherently resilient to such errors, and an error of about 5% in the pixel value may be acceptable in many cases. Even so, we will show that strain causes visible problems in rendered images.

The V_{disp} charging transient is a function of mobility and the applied voltage, V_{data}, and the point of interest on this transient is its value at time t_{row}, when the charging process ends. At a fixed value of t_{row}, we build a linear model that captures the impact of strain on the final voltage value, over various values of V_{data}:

$$V_{disp}^{strain}(t_{row}) = V_{disp}^{0} + k_V V_{data} + k_\mu \mu^{strain} \tag{5}$$

where V_{disp}^{strain} is the voltage level of V_{disp} after incorporating strain-induced mobility variation for a transition from 0 to V_{data}, V_{disp}^{0}, k_V, and k_μ are fitting constants, and μ^{strain} is the mobility under strain.

These models are built at a set of fixed values of t_{row}, and linear interpolation is used to evaluate the model at any intermediate values of t_{row}. Each such model is based on HSPICE simulations using the OPDK. We generate data at 35 points (7 values of V_{data} $\times$ 5 values of μ) at each t_{row} to obtain the function. This is a one-time exercise for a given technology and the cost of characterization is not large.

Combining the fitted linear model with the ability to interpolate at any value of t_{row}, we represent our display voltage model as:

$$V_{disp}^{strain} = f(V_{data}, \mu^{strain}, t_{row}) \tag{6}$$

Although the above model has been characterized for a transition from 0 to V_{data}, it may be used for any transient where the gap between the initial and final values of capacitor voltage is V_{data}. Intuitively, this is because the transition time depends on the RC time constant of the transition and the gap between the initial and final voltage levels. To see this more concretely, we use the RC model in Fig. 6, where R is the equivalent OTFT resistance. Then

$$V_{disp}(t) = V_0 + (V_{data} - V_0)(1 - e^{-\frac{t}{RC_{st}}}) \tag{7}$$

The time required to charge V_{disp} to a voltage $\mathcal{V}$ is

$$t = RC_{st} \cdot \ln \frac{V_{data} - V_0}{V_{data} - \mathcal{V}} \tag{8}$$

For the same charging range $V_{data} - V_0$, the time required to get within $\Delta V = V_{data} - \mathcal{V}$ of the final value is the same. As our result is always determined by the ΔV value (e.g., 1.95mV for half a pixel of accuracy), our model can be used for any initial V_0 and any final V_{data}. Discharge transients are handled using similar principles.

Fig. 8 shows the accuracy of the fitted linear model in Eq. (5) at the 35 sample points, corresponding to 7 values of μ and 5 values of V_{data}. The red dotted line shows the value evaluated from the linear function for V_{disp}^{strain} at $t_{row} = 7.8\mu$s while the blue circles represent the 35 samples. To evaluate the quality of interpolation, we evaluate the interpolation at another 80 points, which differ from the points used to build the model. The error distribution of the error in percentage between the interpolation model in Eq. (6) and the samples

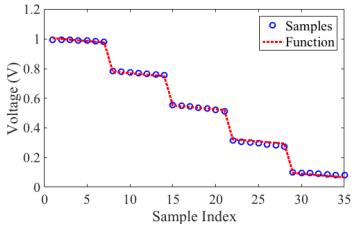

Fig. 8: Accuracy of the fitted function for $V_{disp}^{strain}(t_{row})$.

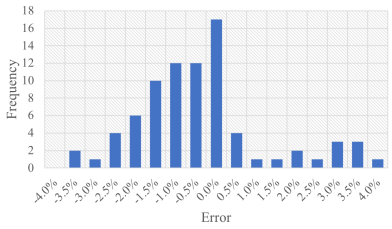

Fig. 9: Error histogram for the interpolation function for V_{disp}^{strain}.

is as shown in Fig. 9. As shown in the figure, the interpolation has a high accuracy while the mean and variance of the interpolation model is -0.34% and 2.69×10^{-4}, respectively.

V. Evaluation of the Analysis Technique

We apply the analysis from the previous sections to present a series of results that show the effect of the extrinsic strain caused by deformations. We consider the deformations in Section II for this evaluation. Note that other types of deformations may also be evaluated, but the intent behind using these specific cases is to mimic the behavior of the display after typical stress tests such as this. A similar approach may be followed to evaluate the degradation in the quality of a displayed image for any other stress test.

We use the SSIM [25], [26], a widely-used metric that measures the structural similarity between two images, to compare rendered images with the ideal. The SSIM metric ranges from -1 to 1, and is

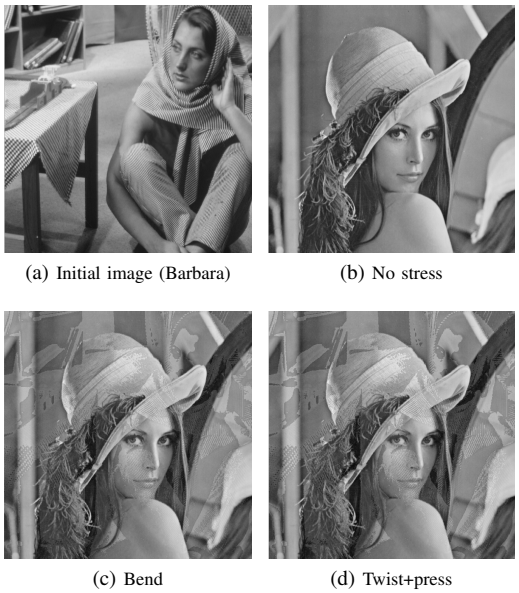

(a) Initial image (Barbara) (b) No stress

(c) Bend (d) Twist+press

Fig. 10: Results for displaying Lena after Barbara.

(a) Girlface (b) Cameraman

(c) Bend (d) Twist+press

Fig. 11: Results for displaying Cameraman after Girlface.

close to 1 when the images are nearly identical. The baseline image in our evaluations is the original image to be rendered.

The image Lena is chosen as the input that provides the inputs V_{data} to all pixels of the display. The initial values of all pixels are based on the image Barbara, as shown in Fig. 10(a), and this corresponds to viewing the display switch from one image (Barbara) to another (Lena). These initial values are the initial voltages V_{disp} across the storage capacitor C_{st} in each pixel. The clock period t_{row} is set to 7.8μs. This value is chosen to ensure that the worst-case error is below 5% in the absence of stress: Fig. 10(b) shows the transition from Barbara to Lena in the strain-free case. Here, the 5% error margin provides excellent rendering at the scale shown.

Next, the same evaluation is repeated when the display undergoes the bend and twist+press deformations (described in Section II), respectively. These results are shown in Fig. 10(c) and (d), respectively. Under strain, the charging/discharging process does not complete fully in the allocated time, t_{row}, and ghosts of the previous picture Barbara can still be distinguished in the result. The SSIM values for these three images are 0.9823 for the strain-free image (b), and 0.6695 and 0.6314 for the images in (c) and (d), respectively.

Another example is shown in Fig. 11. The flexible display is refreshed from picture Girlface as shown in (a), to render the picture Cameraman. The stress-free case is shown in (b), while (c) and (d) show the result for bend and twist+press deformations. The difference between the pictures is very apparent visually, and through the SSIM metrics: 0.9665 for (b), 0.7184 for (c), and 0.6910 for (d). The errors caused by strain can be more significant for displaying videos with frequent refreshes or in a display with more rows.

More SSIM results are summarized in Table II. We shown the results for 15 pictures such as Baboon as shown in the first column with the influence under the strain from the two kinds of deformations. It is assumed that each picture is refreshed from Black, Lena, Barbara and Fingerprint respectively as shown in the first row. It can be found that strain in both deformations can cause significant errors. Larger errors will be caused by more significant strain induced in twist+press deformation. Furthermore, the SSIM result is affected by input pictures. An initial black image will barely affect the structure of the next picture to be displayed, and is less disruptive; however the other three pictures will interfere with the structure of the new image in different ways, depending on the similarity between the images.

TABLE II: Summary of SSIM Results

	Black		Lena		Barbara		Fingerprint	
	SSIM (Bend)	SSIM (T.+p.)	SSIM (Bend)	SSIM (T.+p.)	SSIM (Bend)	SSIM (T.+p.)	SSIM (Bend)	SSIM (T.+p.)
Baboon	0.9878	0.9832	0.8491	0.8137	0.8359	0.8017	0.7358	0.6904
Boat	0.9608	0.9486	0.7990	0.7622	0.7685	0.7324	0.6392	0.5911
Bridge	0.9738	0.9624	0.8801	0.8494	0.8644	0.8312	0.8189	0.7824
Cameraman	0.8225	0.8151	0.6692	0.6341	0.6162	0.5806	0.4217	0.3897
Clown	0.6638	0.6234	0.7873	0.7485	0.7376	0.6964	0.7020	0.6637
Couple	0.9714	0.9619	0.7749	0.7337	0.7883	0.7490	0.6787	0.6340
Crowd	0.9571	0.9358	0.7984	0.7714	0.7638	0.7322	0.7009	0.6715
Feather	0.9490	0.9327	0.3983	0.3448	0.3899	0.3319	0.3538	0.3272
Girlface	0.8049	0.7884	0.7199	0.6814	0.6430	0.6085	0.4820	0.4395
Goldhill	0.9768	0.9650	0.8312	0.7955	0.7748	0.7364	0.7126	0.6718
Pirate	0.9730	0.9615	0.8084	0.7722	0.7564	0.7202	0.6493	0.6084
Plane	0.9953	0.9915	0.8027	0.7813	0.7483	0.7247	0.5376	0.5093
Tank	0.9887	0.9861	0.7258	0.6766	0.7345	0.6930	0.5588	0.4982
Truck	0.9772	0.9702	0.7870	0.7490	0.7394	0.6991	0.5692	0.5202
Zelda	0.9200	0.8980	0.7508	0.7102	0.6850	0.6466	0.5899	0.5510

0.3-0.4 0.4-0.5 0.5-0.6 0.6-0.7 0.7-0.8 0.8-0.9 0.9-1.0

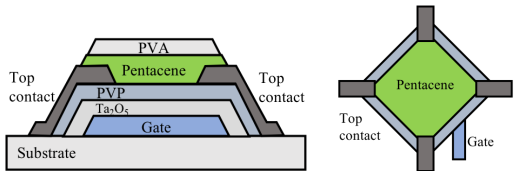

(a) Cross section (b) Top view

Fig. 12: Schematic of the pentacene field-controllable strain sensor based on hybrid gate dielectrics (high-k Ta_2O_5+PVP) [27].

VI. Correcting Strain-Induced Performance Loss

As discussed in Sec. II–IV, the strain induced in the use of the flexible display can cause the mobility degradation of OTFT devices. This mobility degradation can cause errors in the pixel values among the pixels of the flexible display. In this section, we propose two methods to compensate for the errors caused by the extrinsic strain.

Our approach is based on placing compact, flexible strain sensors in another layer added between the *flexible substrate* and *matrix backplane* to sense the presence of an extrinsic strain. Each sensor covers multiple rows and columns of the display array. Because the thickness of the sensor layer is small (100nm) and it is in close proximity to the *matrix backplane* layer and is effective in sensing the strain there.

Data from these sensors is fed back to a controller that applies compensating excitations to maintain image quality. We use the pentacene-semiconductor-based Wheatstone bridge strain sensor whose structure is shown in Fig. 12 [27]. The sensor is fabricated on the flexible substrate. A hybrid film of Ta_2O_5 and PVP is used as the gate dielectric layer and a thin pentacene film acts as the sensing area. A bottom-buried gate electrode controls the carrier channel in the pentacene layer while the other four top contacts are used as the input (the lateral pair) and output (the vertical pair) signals of the strain sensor. The two input contacts of the sensor bridge are used to apply the bias voltage while the output contacts read the output signal, which varies with the change in resistivity induced by the mechanical deformation, and can be translated into the amount of stress/strain and mobility variation.

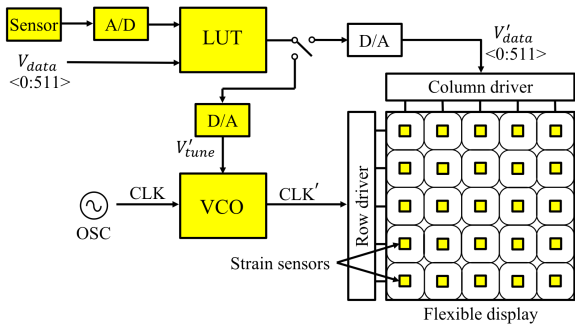

Fig. 13: An architecture showing V_{data} and t_{row} compensation.

From Eq. (6), V_{disp} depends on V_{data}, t_{row}, and μ. Under strain, the voltage waveform may be shifted from the nominal V_{disp} to V'_{disp} even as V_{data} and t_{row} are unchanged, i.e.,

$$V'_{disp} = f(V_{data}, \mu', t_{row}) \tag{9}$$

To make the image immune to strain, we can return V'_{disp} to V_{disp} either by compensating V_{data}, by changing the input pixel values, or by using a longer t_{row}, adjusted using a voltage-controlled (VCO).

$\mathbf{V_{data}}$ compensation: Instead of using the original input pixel value V_{data}, a compensating input V'_{data} is generated with Eq. (9) to make

$$f(V'_{data}, \mu', t_{row}) = V_{disp} \tag{10}$$

Comparing to Eq. (9), a compensating V'_{data} is applied instead of V_{data} to enable the output to reach the target pixel value V_{disp} at time t_{row} under the changed mobility, μ'.

$\mathbf{t_{row}}$ compensation: The charge/discharge time is extended from the nominal value, t_{row}, to a larger value, t'_{row}. Since the mobility degradation reduces the OTFT current, it slows down the charge/discharge process: this compensation allows more to complete the transient.

$$f(V_{data}, \mu', t'_{row}) = V_{disp} \tag{11}$$

The value of t'_{row} is controlled by clock signal (CLK) used for the column driver, and a voltage-controlled oscillator (VCO) [28], which is placed on a separate (nonflexible) board with other control circuits such as row/column drivers, allows its period to be changed.

The architecture for V_{data} and t_{row} compensation is shown in Fig. 13. First, a sensor layer with 10×10 sensors is added between *flexible substrate* and *matrix backplane*. The chosen 10×10 granularity reflects the earlier observation that under normal deformations, the spatial change in strains is gradual. Because the output of the sensor is an analog signal, an analog-to-digital (A/D) converter is added to each strain sensor. The 4-bit feedback-type A/D converters are used here, each of which consists of a 4-bit counter, a 4-bit D/A converter and a comparator; this can also be placed on the board with the drivers and does not need to be flexible. The compensating outputs are provided by a look-up table (LUT), which is implemented with a ROM. The digital data from the strain sensor addresses the LUT, and for each V_{data} value, and compensating output is generated, depending on the compensation method that is used.

$\mathbf{V_{data}}$ compensation: The inputs of the LUT for V_{data} compensation method are the input pixel value for each column and the digital strain value from the nearest strain sensor. The output is the compensating input pixel value V'_{data}. Finally, by applying the compensating input pixel value V'_{data} to the column driver, the accurate output pixel values are expected to show on the flexible display. The LUT takes 12 inputs – the 8-bit V_{data} value and the 4-bit encoding of the strain sensor output from the A/D converter – and outputs the compensated 8-bit V'_{data} value. Thus, the size of the LUT is 4K×8, i.e., 32Kb.

$\mathbf{t_{row}}$ compensation: The input of the LUT for t_{row} compensation approach is the digital strain value from the strain sensor and A/D converter. Since this compensation for t_{row} is applied row-wise, it must be safe for each cell within the row, i.e., the compensating t'_{row} must satisfy the worst-case charge/discharge time for any pixel in the row. This implies that we must consider the maximum strain in the row. Accordingly, the input strain value to the LUT is the maximum value among the strain sensors in the row, and the output V'_{tune} is sent to the VCO to change its frequency.

As before, the LUT uses 12 inputs, corresponding to 8 V_{data} lines 4 sensor data lines. An 8-bit output is provided: because the range of the t_{row} is from 0 to 30μs, this corresponds to a resolution of about 0.1μs in t_{row}. Thus, the capacity requirement for the LUT is the same as for V_{data} compensation, and equals to 32Kb (4K entries×8 bit V'_{tune}). The digital value of V_{tune} is converted to analog form and sent to an 8-bit D/A converter that converts the digital value to an analog input signal for the VCO.

Assuming that both compensation modes are supported, the total overhead of the compensation approach is marked by the yellow blocks in Fig. 13. This includes the 10×10 sensor array, 10×10 A/D converters, a 32Kb LUT, a VCO and a 8-bit D/A converter. As stated above, the flexible sensors are placed in the sensor layer while other circuits are implemented with stable (inflexible) CMOS technology.

VII. Evaluation of the Compensation Scheme

As discussed in Sec. VI, two methods can be used to compensate the error induced by strain: altering V_{data} and changing t_{row} adaptively. The results of V_{data} compensation are as shown in Fig. 14, where the display is refreshed from Barbara to Lena, as in Fig. 10(b). When the compensating input V'_{data} is generated using the V_{data} compensation method as discussed in Sec. VI, the corresponding value of V'_{data} in each pixel would produce the image in (a) if the display were not stressed. The ghosts in this image (which is never rendered in this way, because the display is actually under stress) create a watermark that is the inverse of the case when V_{data} is used on the stressed display. This effectively cancels out the ghosts in the bent picture, and render the ghost-free image in (b). The SSIM result of (b), compared to the perfect Lena image is 0.9546, with the 10×10 spatial sensor resolution being the main accuracy limiter. With 512×512 sensors the scheme can fully compensate the errors and reach a SSIM result equals to 1.

(a) New input V'_{data} (b) Result with compensation

Fig. 14: Results for displaying Lena with V_{data} compensation.

A second method to correct the strain-induced error is through t_{row} compensation, which stretches the clock to lengthen the row charge/discharge time. Fig. 15 shows several results under the bend-induced strain as the display changes from Barbara to Lena, as before. The four images to SSIM values of 0.65, 0.70, 0.80, and 0.99. The corresponding values of t_{row} are 3.7μs, 12.3μs, 21.4μs, and 29.1μs, respectively, in (a), (b), (c), and (d). It can be seen that when t_{row} is large enough, the result is very close to the input. As compared to V_{data} compensation, this method requires a ∼4× larger value of

(a) SSIM=0.65, t_{row}=3.7μs (b) SSIM=0.70, t_{row}=12.3μs

(c) SSIM=0.80, t_{row}=21.4μs (d) SSIM=0.99, t_{row}=29.1μs

Fig. 15: Results for displaying Lena with t_{row} compensation.

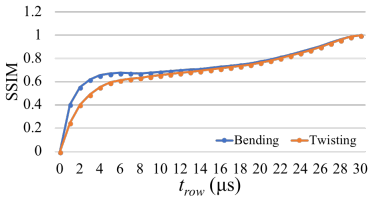

Fig. 16: Relationship between SSIM and t_{row}.

t_{row} for comparable quality. As seen in Fig. 7, the amount of time required to reach high levels of accuracy can increase greatly because the V_{disp} curve has a very low slope late in its transient. This increase in t_{row} may be acceptable in some applications and not others.

For a more fine-grained range of t_{row}, Fig. 16 shows the relationship between SSIM results and t_{row}, where the blue line represents the curve with the bend-induced strain while the orange line is the relationship under the deformation of twist+press, both from Section II. As expected, a better quality result can be obtained with longer charge/discharge time, at the cost of slower rendering.

As compared to V_{data} compensation, t_{row} compensation significantly reduces the number of LUT lookups. The former requires 512×512 lookups, one for each pixel. In t_{row} compensation, each row of the strain sensor array covers multiple rows of the display array, and the largest strain in any row of the sensor array determines the t_{row} value for all display rows that it covers. Thus, this scheme requires only 10 lookups to the LUT. However, to reach high quality, t_{row} compensation needs a longer refresh time t'_{row}, unlike V_{data} compensation, which keeps t_{row} unchanged.

VIII. Conclusion

We have presented a performance analysis of flexible displays while incorporating the impact of realistic extrinsic strain. It is seen that deformations can significantly affect the quality of an image on the OTFT display. Based on data from an array of flexible strain sensors, two compensation methods are proposed: V_{data} compensation, which adjusts the data value sent to each pixel, and t_{row} compensation, which alters the time allowed for charging/discharging each pixel. V_{data} compensation can be used in scenarios in which a fixed t_{row} is preferred, while t_{row} compensation can be used for applications where fewer ROM accesses are preferred, the system can tolerate a change in t_{row}, and slightly lower quality results are acceptable if the acceptable increase in t_{row} is limited.

References

[1] K. Nomoto, *et al.*, "A High-Performance Short-Channel Bottom-Contact OTFT and its Application to AM-TN-LCD," *IEEE Transactions on Electron Devices*, vol. 52, no. 7, pp. 1519–1526, 2005.

[2] J.-h. Lee, *et al.*, "World's Largest (15-inch) XGA AMLCD Panel Using IGZO Oxide TFT," in *Proc. SID Symposium*, pp. 625–628, 2008.

[3] C. Wang, *et al.*, "User-Interactive Electronic Skin for Instantaneous Pressure Visualization," *Nature Materials*, vol. 12, no. 10, p. 899, 2013.

[4] E. Cantatore, *Applications of Organic and Printed Electronics: A Technology-Enabled Revolution*. New York, NY: Springer, 2013.

[5] J. Burghartz, *Ultra-Thin Chip Technology and Applications*. New York, NY: Springer, 2010.

[6] D. E. Schwartz, *et al.*, "Flexible Hybrid Electronic Circuits and Systems," *IEEE Journal on Emerging and Selected Topics in Circuits and Systems*, vol. 7, no. 1, pp. 27–37, 2017.

[7] T. Someya, *et al.*, "A Large-Area, Flexible Pressure Sensor Matrix with Organic Field-Effect Transistors for Artificial Skin Applications," *Proc. National Academy of Sciences of the United States of America*, vol. 101, no. 27, pp. 9966–9970, 2004.

[8] W. Zhang, *et al.*, "A 1V Printed Organic DRAM Cell Based on Ion-Gel Gated Transistors with a Sub-10nW-per-Cell Refresh Power," in *Proc. IEEE Solid-State Circuits Conference*, pp. 326–328, 2011.

[9] C. Reese, *et al.*, "Organic Thin Film Transistors," *Materials Today*, vol. 7, no. 9, pp. 20–27, 2004.

[10] H. Klauk, "Organic Thin-Film Transistors," *Chemical Society Reviews*, vol. 39, no. 7, pp. 2643–2666, 2010.

[11] D.-U. Jin, *et al.*, "World-Largest (6.5) Flexible Full Color Top Emission AMOLED Display on Plastic Film and Its Bending Properties," in *Proc. SID Symposium*, pp. 983–985, 2009.

[12] A. N. Sokolov, *et al.*, "Mechanistic Considerations of Bending-Strain Effects within Organic Semiconductors on Polymer Dielectrics," *Advanced Functional Materials*, vol. 22, no. 1, pp. 175–183, 2012.

[13] C.-H. Tu, *et al.*, "Flexible AMOLED Displays with Bending Interactive Interface," in *Proc. SID Symposium*, pp. 1048–1051, 2016.

[14] P. Cosseddu, *et al.*, "Strain Sensitivity and Transport Properties in Organic Field-Effect Transistors," *IEEE Electron Device Letters*, vol. 33, no. 1, pp. 113–115, 2012.

[15] S. Logothetidis, *Handbook of Flexible Organic Electronics: Materials, Manufacturing and Applications*. Elsevier, Cambridge, UK, 2015.

[16] B. Bensaid, *et al.*, "Reliability of OTFTs on Flexible Substrate: Mechanical Stress Effect," *The European Physical Journal–Applied Physics*, vol. 55, no. 2, pp. 23907–1–23907–5, 2011.

[17] T. Sekitani, *et al.*, "Submillimeter Radius Bendable Organic Field-Effect Transistors," *Journal of Non-Crystalline Solids*, vol. 352, no. 9-20, pp. 1769–1773, 2006.

[18] M. Noda, *et al.*, "An OTFT-Driven Rollable OLED Display," *Journal of the Society for Information Display*, vol. 19, no. 4, pp. 316–322, 2011.

[19] Z. Bao, *et al.*, "Soluble and Processable Regioregular Poly (3-hexylthiophene) for Thin Film Field-Effect Transistor Applications with High Mobility," *Applied Physics Letters*, vol. 69, no. 26, pp. 4108–4110, 1996.

[20] S. D. Brotherton, *Introduction to Thin Film Transistors: Physics and Technology of TFTs*. Cham, Switzerland: Springer, 2013.

[21] P. Pingel and D. Neher, "Comprehensive Picture of p-Type Doping of P3HT with the Molecular Acceptor F_4TCNQ," *Physical Review B*, vol. 87, no. 11, p. 115209, 2013.

[22] C. S. Smith, "Piezoresistance Effect in Germanium and Silicon," *Physical Review*, vol. 94, no. 1, p. 42, 1954.

[23] H. Gleskova, *et al.*, "Field-Effect Mobility of Amorphous Silicon Thin-Film Transistors Under Strain," *Journal of Non-Crystalline Solids*, vol. 338, pp. 732–735, 2004.

[24] "Organic Process Design Kit." http://opdk.umn.edu.

[25] Z. Wang, *et al.*, "Image Quality Assessment: From Error Visibility to Structural Similarity," *IEEE Transactions on Image Processing*, vol. 13, no. 4, pp. 600–612, 2004.

[26] S. S. Channappayya, *et al.*, "Rate Bounds on SSIM Index of Quantized Images," *IEEE Transactions on Image Processing*, vol. 17, no. 9, pp. 1624–1639, 2008.

[27] S. Jung, *et al.*, "Pentacene-Based Low-Voltage Strain Sensors with PVP/Ta_2O_5 Hybrid Gate Dielectrics," *IEEE Transactions on Electron Devices*, vol. 57, no. 2, pp. 391–396, 2010.

[28] M. Tiebout, *Low Power VCO Design in CMOS*. Berlin, Germany: Springer, 2006.